Synthesis, Characterization, Antioxidant Activities, and DNA-Binding Studies of (*E*)-*N*′-[1-(Pyridin-2-yl)ethylidene]isonicotinohydrazide and Its Pr(III) and Nd(III) Complexes

Zhong-Yan Hao, Qi-Wan Liu, Jun Xu, Lei Jia, and Shao-Bai Li*

College of Chemistry and Chemical Engineering, State Key Laboratory of Applied Organic Chemistry, Lanzhou University; Lanzhou 730000, P. R. China.

Received December 23, 2009; accepted June 20, 2010; published online July 13, 2010

A new ligand, (*E*)-*N*′-[1-(pyridin-2-yl)ethylidene]isonicotinohydrazide (HL), was prepared by condensation of 2-acetylpyridine and isonicotinohydrazide in ethanol. Its two lanthanide(III) complexes, $[Nd^{III}(L)_2(NO_3)(CH_3OH)_2]\cdot CH_3CH_2OH$ (1), and $[Pr^{III}(L)_2(NO_3)(CH_3OH)_2]\cdot CH_3CH_2OH$ (2), have been synthesized and characterized on the basis of element analyses, molar conductivities and IR spectra. The structure of complex 2 has been confirmed by X-ray diffraction. In addition, the DNA-binding properties of the two complexes have been investigated by electronic absorption spectroscopy, fluorescence spectroscopy, circular dichroic (CD) spectroscopy and viscosity measurements. The experimental results suggest that the two complexes bind to DNA *via* a groove binding mode, and the binding affinity of complex 2 is higher than that of complex 1. Furthermore, the antioxidant activities (superoxide and hydroxyl radical) of the ligand and its metal complexes were determined by spectrophotometry methods *in vitro*. These complexes were found to possess potent antioxidant activity and be superior to standard antioxidant like mannitol.

Key words crystal structure; Pr(III) complex; groove binding; antioxidant activity

It is well-known that Schiff bases play important role in bioinorganic chemistry and their metal complexes have been studied extensively for decades. These interesting ligand systems contain different donor sites in heterocyclic rings, *e.g.*, NNO or NNS, which give rise to the architectural beauty of these coordination complexes.[1)] Among the ligand systems, hydrazide and hydrazone occupy important places because transition metal complexes of these ligands have been developed due to their chelating capability, structural flexibility, interesting electrical as well as magnetic properties, and various pharmacological activities, such as antibacterial, antitumoral, antiviral, antimalarial, and antituberculosis actions.[2,3)]

Investigation of molecular complexes of lanthanide ions has attracted significant attention, owing to their broad ranging fluorescent applications in biochemistry, material chemistry, medicine and so forth.[4—6)] However, there have been only a few DNA-binding investigations of such complexes have been relatively few. Because the interaction between metal complexes and DNA is closely related to their potential biological and pharmaceutical activities, studies on the DNA-binding of metal complexes are very important in the development of new therapeutic reagents and DNA molecular probes.[7,8)] Various coordination compounds of aroylhydrazones have been reported to act as enzyme inhibitors and are useful due to their pharmacological applications.[9,10)]

Here, we synthesized (*E*)-*N*′-[1-(2-pyridinyl)ethylidene]-isonicotinohydrazide (HL) and prepared its two of its lanthanide(III) complexes (Chart 1). The DNA-binding properties and antioxidant activities of the two lanthanide(III) complexes with HL are reported herein.

Experimental

Materials Nitroblue tetrazolium (NBT), methionine (MET), vitamin B_2 ($VitB_2$), calf thymus DNA (CT-DNA) and ethidium bromide (EB) were obtained from Sigma Chemical Co. All experiments involving interaction of the complexes with CT-DNA were carried out in doubly distilled water buffer containing 5 mM Tris [Tris(hydroxymethyl)-aminomethane] and 50 mM NaCl, and adjusted to pH 7.2 with hydrochloric acid. The DNA concentrations of the solutions were determined from their UV absorption at 260 nm using the molar absorption coefficient $\varepsilon_{260}=6600\,mol^{-1}\,cm^{-1}$. DNA Purity was checked by monitoring the ratio of the absorbance at 260 nm to that at 280 nm. The solution gave a ratio of $A_{260}/A_{280}>1.80$, indicating that DNA was sufficiently free from protein.[11)]

Physical Measurements The UV–vis absorption measurements were conducted by using a Varian Cary 100 spectrophotometer equipped with quartz cells. All fluorescence emission spectra were measured using a Hitachi F-4500 spectrofluorophotometer equipped with a xenon lamp source and a quartz cell of 5 cm path length. Viscosity experiments were carried out on an Ubbelodhe viscometer. The circular dichroic (CD) spectra were recorded on a Jasco J-810 spectropolarimeter. The ^{1}H-NMR spectra were recorded with a Bruker ACF300 FT-NMR instrument using tetramethylsilane (TMS) as an internal reference in D_2O for the ligand. Electrospray ionization (ESI) mass spectra were recorded on a Finnigan MAT LCQ mass spectrometer using the syringe pump method. High resolution-mass spectra (HR-MS) were obtained by the ESI ionization sources. All conductivity measurements were performed in *N*,*N*′-dimethyl formamide (DMF) with a DDS-11A conductor at 25 °C. The antioxidant activities were tested on a 721E spectrophotometer (Shanghai Analytical Instrument Factory, China).

DNA Binding Experiment Methods Absorption titration experiments were performed by fixing the concentrations of complexes **1** and **2** as constant at 10 μM while varying the concentration of CT-DNA (10^{-4} mol/l). Fitting was completed using an Origin 6.0 spreadsheet, where the values of the binding constants K_b were calculated. Fluorescence spectra of the competitive binding experiments were obtained by maintaining the EB and CT-DNA concentrations at 3 μM and 30 μM, respectively, while increasing the concentrations of the complexes.

Viscosity experiments were carried out on an Ubbelodhe viscometer, im-

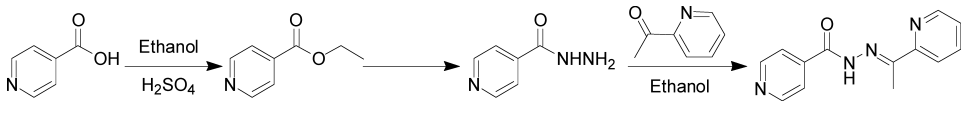

Chart 1. Synthesis Route of the Ligand

* To whom correspondence should be addressed. e-mail: bsli@lzu.edu.cn

mersed in a thermostated water-bath maintained at 25.0±0.1 °C. Titrations were performed for the complexes (1—6 μM), and each complex was introduced into DNA solution (50 μM) present in the viscometer. Flow time was measured with a digital stopwatch and each sample was measured three times and an average flow time was calculated.

The CD spectra of DNA were recorded on a Jasco J-810 spectropolarimeter at 25.0±0.1 °C. Each sample solution was scanned in the range of 200—350 nm. The CD spectrum, which represented the average of three scans, was generated from which the buffer background had been subtracted.

X-Ray Crystallography A suitable yellow single crystal of complex **2** with dimensions of 0.40×0.20×0.10 mm^3 was mounted in a sealed tube for data collection performed in a Bruker AXS SMART CCD diffractometer equipped with a graphite-monochromatic Mo$K\alpha$ radiation (λ=0.71073 Å) at 223(2) K. Unit cell dimensions were obtained with least-squares refinements. The program SMART was used to collect the intensity data,[12] SAINT for integration of the intensity,[12] SADABS for absorption correction and SHELXTL for structure solution and refinements on F^2.[13,14] The phenyl ring was disordered into two positions with occupancy ratio 63 : 37. There were several residual peaks which were too weak and therefore could not be characterized. An H atom of N3 was located from different maps and refined with restraints in bond length and parameters. The H atoms of the solvent molecules were not located. The whole complex **2** was generated by the two fold rotation. One half of ethanol was situated at the centre of symmetry. The H atom of methanol was located from a different map and refined with restraint in bond length. The C and O atoms of the disordered ethanol were not refined ansiotropically because the thermal parameters did not behave well due to the disorder and overlapping. Selected crystallographic data and structure refinement parameters of complex **2** are summarized in Table 1, where selected bond distances and angles are summarized in Table 2.

Synthesis of the Ligand and the Complexes The ligand HL was prepared as described previously.[15] In short, HL was obtained by the condensation of 2-acetylpyridine and isonicotinohydrazide in ethanol solution with the addition of several drops of conc. HCl. IR (KBr) cm^{-1}: ν(NH) 3189, ν(C=O) 1671, ν(C=N) 1548. Complex **1** was prepared as follows. $Nd(NO_3)_3\cdot 6H_2O$ (219.1 mg, 0.5 mmol) in ethanol (10 ml) was added to the solution containing the ligand (240 mg, 1 mmol) in methanol (10 ml). The mixture was stirred for 12 h to form a precipitate of Nd(III) complex formed. The precipitate was separated by centrifugation and washed three times with ethanol and one time with ether, and then dried *in vacuo*. *Anal.* Calcd for $C_{30}H_{36}N_9O_8Nd$: C, 45.33; H, 4.56; N, 15.86, Found: C, 45.50; H, 4.67; N, 15.99. IR (KBr) cm^{-1}: ν(C=O) 1570, ν(C=N) 1512. The Pr(III) complex was synthesized in the same way. Slow evaporation of the mixed methanol/ethanol solution containing Pr(III) complex **2** afforded a yellow single crystal which is suitable for X-ray diffraction. *Anal.* Calcd for $C_{30}H_{36}N_9O_8Pr$: C, 45.52; H, 4.58; N, 15.93, Found: C, 45.65; H, 4.69; N, 15.70. IR (KBr) cm^{-1}: ν(C=O) 1576, ν(C=N) 1515. HR-MS (ESI) Calcd for $[PrL_2]^+$: 619.0942; $[PrL_2+CH_3OH]^+$: 651.1204; $[PrL_2+CH_3COCH_3]^+$: 677.1361; $[PrL_2+2\times(CH_3COCH_3)]^+$: 735.1779. Found $[PrL_2]^+$: 619.1022; $[PrL_2+CH_3OH]^+$: 651.1260; $[PrL_2+CH_3COCH_3]^+$: 677.1347; $[PrL_2+2\times(CH_3COCH_3)]^+$: 735.1678, L=$C_{13}H_{11}N_4O^-$. The complexes are soluble at room temperature in ethanol, methanol, DMF and dimethyl sulfoxide (DMSO).

Superoxide Radical Scavenging Assay Superoxide radicals ($O_2^{-\cdot}$) were generated *in vitro* using a non-enzymatic system and determined spectrophotometrically by a NBT photoreduction method whicn wae a slight modification of a method described previously.[16—19] The amount of $O_2^{-\cdot}$ and suppression ratio for $O_2^{-\cdot}$ can be calculated by measuring the absorbance at 560 nm. Light was avoided while preparing solutions of MET, VitB_2 and NBT were prepared avoiding light. The tested compounds were dissolved in DMF. The assay mixture, in a total volume of 5 ml, contained MET (10 mM), NBT (46 μM), VitB_2 (3.3 μM), the tested compound (5—20 μM) and a phosphate buffer (67 mM, pH 7.8). After illuminating with a fluorescent lamp at 30 °C for 10 min, the absorbance of the samples (A_i) was measured at 560 nm. The sample without the tested compound was used as control and its absorbance was A_0. All experimental results were expressed as the mean±standard deviation (S.D.) of triplicate determinations. The suppression ratio for $O_2^{-\cdot}$ was calculated from the following expression:

$$\text{suppression ratio } (\%) = A_0 - A_i/A_0 \times 100 \quad (1)$$

Drug activity was expressed as the 50% inhibitory concentration (IC_{50}). IC_{50} values were calculated from regression lines where: x was the tested compound concentration in mM and y was percent inhibition of the tested compounds.

Table 1. Crystal and Experimental Data for Complex **2**

Empirical formula	$C_{30}H_{34}N_9O_8Pr$
Formula weight	789.57
Temperature	223(2) K
Wavelength	0.71073 Å
Crystal system	Monoclinic
Space group	$P2/n$
Unit cell dimensions (Å, °)	
a	11.6516(8)
b	11.2406(8)
c	12.9195(9)
β	100.034(2)
Volume (Å^3)	1666.2(2)
Z	2
D_{calcd} (g/cm^3)	1.574
Absorption coefficient (mm^{-1})	1.525
F(000)	800
Range of $h\,k\,l$	−15/14, −14/14, −12/16
Reflections collected	12846
Data/restraints/parameters	3823/4/222
Max. and min. transmission	0.8625, 0.5807
Goodness-of-fit on F^2	1.088
Final R indices [$I>2\sigma(I)$]	$R1$=0.0347, $wR2$=0.0845
Largest diff. peak and hole (Å^{-3})	1.395, −0.776

Table 2. Selected Bond Distances and Angles (Å, °) for Complex **2**

Pr(1)–O(1)	2.414(2)	Pr(1)–O(2)	2.624(2)
Pr(1)–O(1)$^{a)}$	2.415(2)	Pr(1)–N(2)$^{a)}$	2.687(3)
Pr(1)–O(4)	2.558(2)	Pr(1)–N(2)	2.687(3)
Pr(1)–O(4)$^{a)}$	2.558(2)	Pr(1)–N(1)$^{a)}$	2.707(2)
Pr(1)–O(2)$^{a)}$	2.624(2)	Pr(1)–N(1)	2.707(2)
O(1)–Pr(1)–O(1)$^{a)}$	147.3(2)	O(1)–Pr(1)–O(4)	83.20(7)
O(1)$^{a)}$–Pr(1)–O(4)	70.51(7)	O(1)–Pr(1)–O(4)$^{a)}$	70.51(7)
O(1)$^{a)}$–Pr(1)–O(4)$^{a)}$	83.20(7)	O(4)–Pr(1)–O(4)$^{a)}$	73.3(2)
O(1)–Pr(1)–O(2)$^{a)}$	129.19(8)	O(1)$^{a)}$–Pr(1)–O(2)$^{a)}$	83.16(8)
O(4)–Pr(1)–O(2)$^{a)}$	139.92(8)	O(4)$^{a)}$–Pr(1)–O(2)$^{a)}$	134.13(8)
O(1)–Pr(1)–O(2)	83.17(8)	O(1)$^{a)}$–Pr(1)–O(2)	129.18(8)
O(4)–Pr(1)–O(2)	134.13(8)	O(4)$^{a)}$–Pr(1)–O(2)	139.92(8)
O(2)$^{a)}$–Pr(1)–O(2)	48.9(2)	O(1)–Pr(1)–N(2)$^{a)}$	123.62(8)
O(1)$^{a)}$–Pr(1)–N(2)$^{a)}$	59.99(8)	O(4)–Pr(1)–N(2)$^{a)}$	120.07(8)
O(4)$^{a)}$–Pr(1)–N(2)$^{a)}$	69.58(8)	O(2)$^{a)}$–Pr(1)–N(2)$^{a)}$	65.66(7)
O(2)–Pr(1)–N(2)$^{a)}$	103.86(7)	O(1)–Pr(1)–N(2)	59.99(8)
O(1)$^{a)}$–Pr(1)–N(2)	123.62(8)	O(4)–Pr(1)–N(2)	69.58(8)
O(4)$^{a)}$–Pr(1)–N(2)	120.07(8)	O(2)$^{a)}$–Pr(1)–N(2)	103.86(7)
O(2)–Pr(1)–N(2)	65.66(7)	N(2)$^{a)}$–Pr(1)–N(2)	169.1(2)
O(1)–Pr(1)–N(1)$^{a)}$	72.99(8)	O(1)$^{a)}$–Pr(1)–N(1)$^{a)}$	118.89(7)
O(4)–Pr(1)–N(1)$^{a)}$	144.57(8)	O(4)$^{a)}$–Pr(1)–N(1)$^{a)}$	74.23(8)
O(2)$^{a)}$–Pr(1)–N(1)$^{a)}$	74.72(8)	O(2)–Pr(1)–N(1)$^{a)}$	69.35(8)
N(2)$^{a)}$–Pr(1)–N(1)$^{a)}$	58.95(8)	N(2)–Pr(1)–N(1)$^{a)}$	116.84(8)
O(1)–Pr(1)–N(1)	118.89(7)	O(1)$^{a)}$–Pr(1)–N(1)	72.99(8)
O(4)–Pr(1)–N(1)	74.23(8)	O(4)$^{a)}$–Pr(1)–N(1)	144.57(8)
O(2)$^{a)}$–Pr(1)–N(1)	69.35(8)	O(2)–Pr(1)–N(1)	74.72(8)
N(2)$^{a)}$–Pr(1)–N(1)	116.84(8)	N(2)–Pr(1)–N(1)	58.95(8)
N(1)$^{a)}$–Pr(1)–N(1)	140.5(2)		

Symmetry code: *a*) $-x+1/2, y, -z+3/2$.

Hydroxyl Radical Scavenging Assay The hydroxyl radicals ($OH^{\cdot}$) in aqueous media were generated through the Fenton system.[20] The solution of the tested compound was prepared with DMF. The 5 ml assay mixture contained the following reagents: safranin (11.4 μM), ethylenediaminetetraacetic acid (EDTA)-Fe(II) (40 μM), H_2O_2 (1.76 mM), the tested compound (2—15 μM) and a phosphate buffer (67 mM, pH 7.4). The assay mixtures were incubated at 37 °C for 30 min in a water bath and then the absorbance was measured at 520 nm. All tests were run in triplicate and are expressed as the mean±standard deviation (S.D.).

The suppression ratio for $OH^{\cdot}$ was calculated from the following expression:

$$\text{suppression ratio } (\%) = [(A_i - A_0)/(A_c - A_0)] \times 100 \quad (2)$$

(Where A_i=the absorbance in the presence of the tested compound; A_0=the absorbance in the absence of the tested compound; A_c=the absorbance in the absence of the tested compound, EDTA-Fe (II), H_2O_2.)

Results and Discussion

Synthesis and General Properties Complexes **1** and **2** were prepared in high yield from reactions of the Schiff base ligand HL in the presence of $Pr(NO_3)_3 \cdot 6H_2O$ or $Nd(NO_3)_3 \cdot 6H_2O$. The stability of the two complexes in an aqueous solution had been studied by observing the UV–vis spectrums and estimating the molar conductivities at different time intervals for any possible change. The tested complexes were prepared in methanol and for experiments freshly diluted in phosphate buffer system (at pH 7.4, 7.8). Next, the UV–vis spectra and molar conductivities were examined at different time intervals. These investigations revealed that the UV–vis spectra had remained unaltered for the solutions and there were no obvious changes in the molar conductivity values of either freshly prepared solutions or those used throughout the entire experiment (24 h). This indicated that the complexes are quite stable in solution. The molar conductivity data were in accordance with the non-electrolyte.

IR Spectra The IR spectra of the two complexes are very similar. The ν(C=O) of the free ligand are at 1671 cm^{-1}, for complexes **1** and **2** this peak shifted to 1570 and 1576 cm^{-1}, and the ν(ligand–complexes) is equal to 101 and 95 cm^{-1}, thus indicating that the O atom of C=O is involved in coordination to the metal ion. The band at 1548 cm^{-1} for the free ligand is assigned to the ν(C=N) stretch, which shifts to 1512 and 1515 cm^{-1} for complex **1** and **2**, indicating that the N atom of C=N is involved in coordination to the metal ion. The vibrations ν(N–H) had disappeared in the spectra of the two complexes indicating that the ligand is deprotonated. The new bands at 561 and 555 cm^{-1} for complexes **1** and **2** are assigned to ν(M–O), and the weak peaks at 470 and 476 cm^{-1} for complexes **1** and **2** are assigned to ν(M–N), respectively.[21,22]

Crystal Structure Complex **2** crystallized in the monoclinic space group $P2/n$. The X-ray crystal structure of the $[Pr^{III}(L)_2(NO_3)(CH_3OH)_2] \cdot CH_3CH_2OH$ with atom numbering chart is presented as an ORTEP figure in Fig. 1. The crystal structure revealed that the discrete molecules of $[Pr(C_5H_4N–C(CH_3)=N–N=C(O)–C_5H_4N)_2]$ are held together by very weak van der Waal's forces. Under the reaction condition, the ligand molecule tautomerises from the ketonic $[C_5H_4N–C(CH_3)=N–NH–C(O)–C_5H_4N]$ to enolic form $[C_5H_4N–C(CH_3)=N–N=C(OH)–C_5H_4N]$. These two ligand molecules are coordinated to the Pr(III) centre in the monoanionic form after deprotonation of the enolic oxygen atom, being coordinated to Pr(III) *via* the pyridine and hydrazone nitrogen atoms as well as *via* the α-oxyazine oxygen. Their coordination in the α-oxyazine form results in the formation of four 5-membered chelate rings around the Pr(III) centre. The experimental parameters of the single-crystal X-ray analysis of the Pr complex **2** indicate that the mononuclear Pr atom is surrounded by ten coordinated donor atoms. Six of them belong to two deprotonated ligands, two to the bidentate nitrate group and two to coordinated methanol molecules (with all the Pr–O bond lengths rang from 2.414(2) Å to 2.624(2) Å and the O–Pr–O angles ranging from 48.9(2) to 147.3(2)°). The coordination polyhedron around Pr^{3+} is a distorted bicapped square antiprism, as shown in Fig. 2.

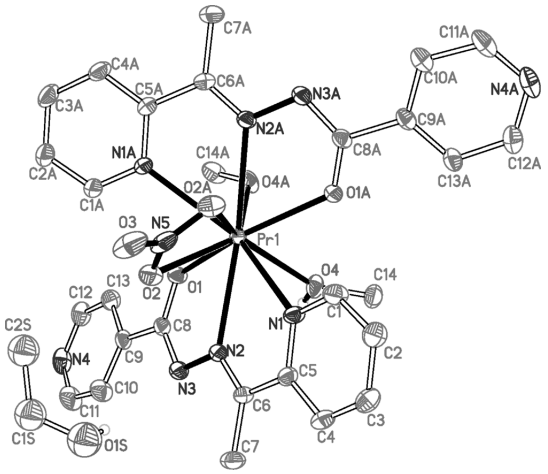

Fig. 1. Molecular Structure of the Pr(III) Complex Showing 30% Probability Displacement Ellipsoids and the Atom-Numbering Chart

Hydrogen atoms attached to carbon atoms have been omitted for clarity.

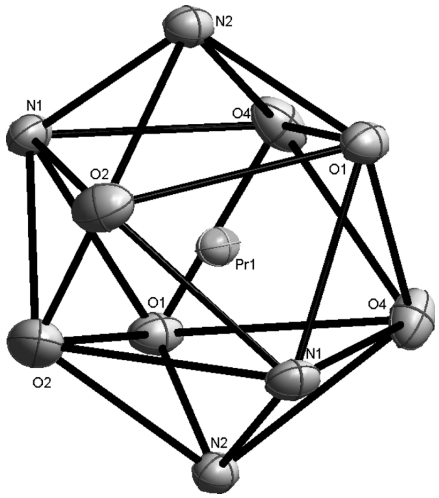

Fig. 2. Coordination Polyhedron of Complex **2**

DNA-Binding Studies. Electronic Absorption Titration Electronic absorption spectroscopy is universally employed to examine the binding mode of DNA with small molecules. The ligand has no effect on the absorption of DNA solutions. The absorption spectra of complexes **1** and **2** in the absence and presence of CT DNA are given in Figs. 3a and b. In the absence of CT DNA, the UV–Vis absorption spectra of complex **1** has three well-solved bands at λ_{max}=206, 263 and 344 nm, while complex **2** has three bands at λ_{max}=205, 265 and 342 nm. With increasing DNA concentration, the absorption bands around 205 and 265 nm of the two complexes show obvious decreases in molar absorptivity (hypochromism) as well as marked bathochromism. In order to study the binding ability of the compounds with DNA quantitatively, the binding constant K_b was determined using the following Eq. 3,[23]

$$[DNA]/(\varepsilon_a-\varepsilon_f)=[DNA]/(\varepsilon_b-\varepsilon_f)+1/K_b(\varepsilon_b-\varepsilon_f) \quad (3)$$

where [DNA] is the concentration of DNA in base pairs, ε_a, ε_f, and ε_b are the apparent extinction coefficient correspon-

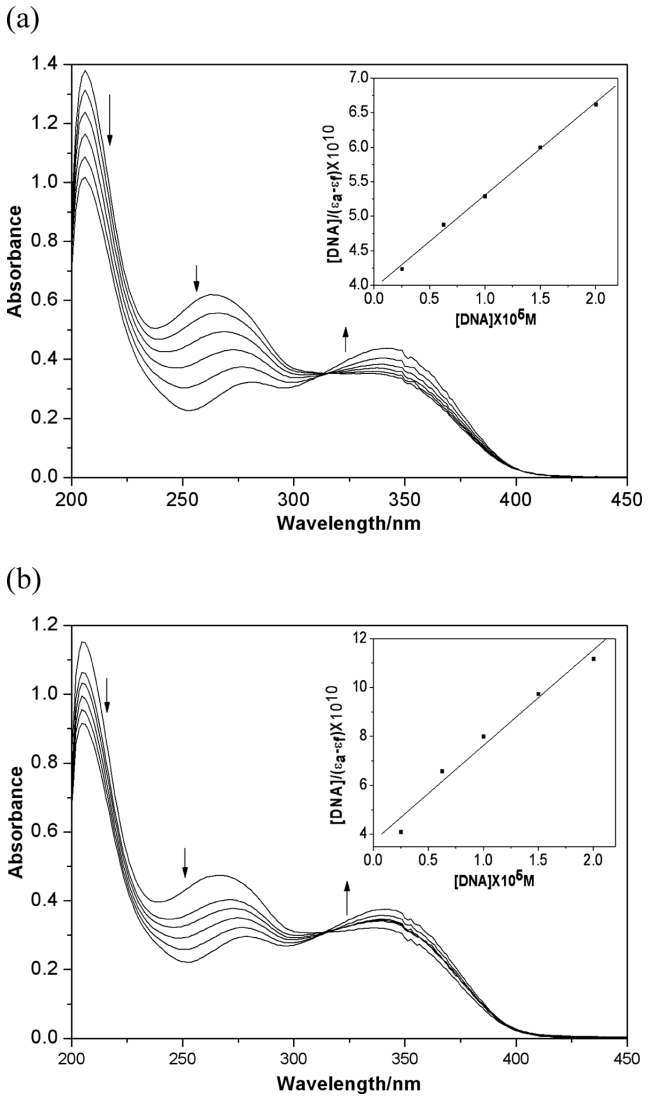

Fig. 3. Electronic Spectra of the Complex **1** (a) and Complex **2** (b) in the Presence of 0—20 μM CT-DNA

Arrow shows the absorbance intensity changes upon increasing DNA concentration. Inset: plots of [DNA]/($\varepsilon_a-\varepsilon_f$) *vs.* [DNA] for the titration of compound.

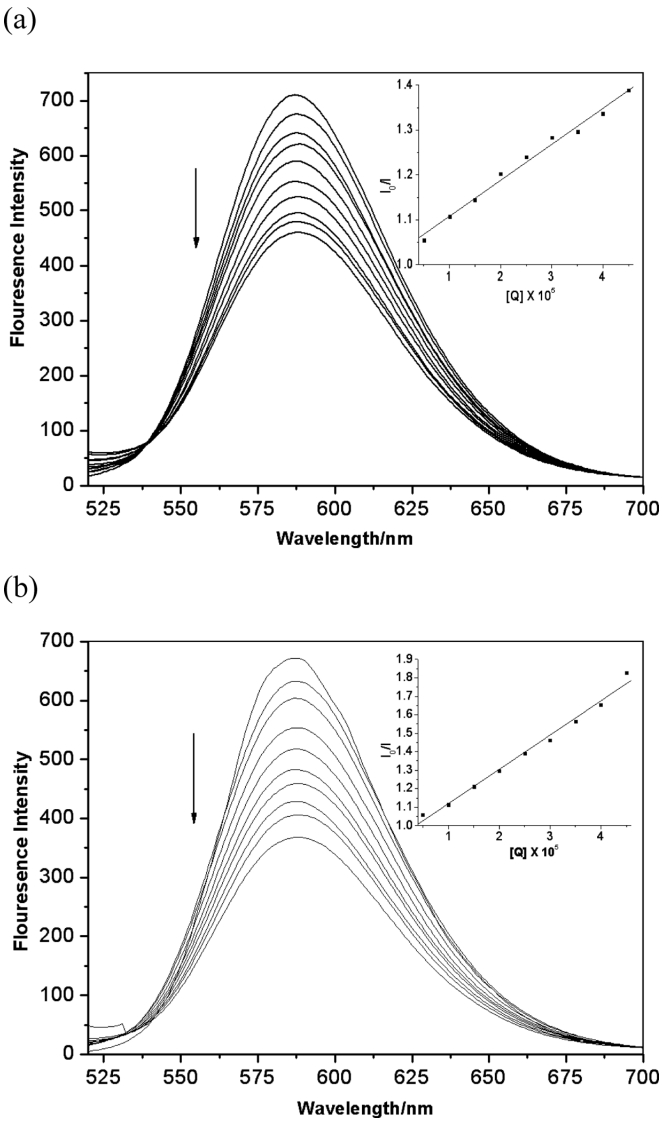

Fig. 4. Emission Enhancement Spectra of Complexes **1** (a) and **2** (b) in the Presence of 0—50 μM CT-DNA

Arrow shows the emission intensities changes upon increasing the DNA concentration.

ding to A_{obsd}/[M], the extinction coefficient for the free compound and the extinction coefficient for the compound in the fully bound form, respectively. In plots of [DNA]/($\varepsilon_a-\varepsilon_f$) *versus* [DNA], K_b is given by the ratio of the slope to the intercept, as shown in Fig. 3.

The binding constants K_b for complexes **1** and **2** were found to be $4.31\times10^4\,M^{-1}$ and $1.24\times10^5\,M^{-1}$, respectively. The results indicate that the binding strength of complex **2** is stronger than that of complex **1**. The K_b value obtained here is lower than that reported for classical intercalator (for ethidium bromide and [Ru(phen)DPPZ] whose binding constants have been found to be in the order of 10^6—10^7 M).[24,25] Such a change in λ_{max} and the observed binding constant is more in keeping with the groove binding with DNA, as observed in the literature.[26,27]

Fluorescence Spectra Further support for the complexes binding to DNA was given through the competitive binding experiment. EB is a conjugate planar molecule. Its fluorescence intensity is very weak, but the intensity greatly increases when EB is intercalated into DNA. When a second ligand is added, it could compete with EB for DNA binding sites and then a decrease in the fluorescence intensity is observed. Therefore EB can be used as a common fluorescent probe for DNA structure and has been employed in investigations of the mode and the process of metal complex binding to DNA.[28]

The emission spectra of the DNA–EB system in the presence of increasing amounts of complexes **1** and **2** are shown in Fig. 4. The fluorescence intensity of EB at 584 nm showed a remarkable decreasing trend with increasing concentrations of the complexes, indicating that some EB molecules are released from EB–DNA after an exchange with the complexes which results in the fluorescence quenching of EB. This may be due either to the metal complex competing with EB for the DNA binding sites and thus displacing the EB (whose fluorescence is enhanced upon DNA binding) or it could be a more direct quenching interaction on the DNA itself. We assume it is the former which implies that complexes **1** and **2** can bind more strongly to DNA than EB.

According to the classical Stern–Volmer Eq. 4,[29]

$$F_0/F=1+K_q[Q] \quad (4)$$

where F_0 and F represent the emission intensity in the absence and presence of quencher, respectively, K_q is a linear Stern–Volmer quenching constant and $[Q]$ is the quencher concentration. The quenching plots illustrate that the quenching of EB bound to DNA by the complexes is in good agreement with the linear Stern–Volmer equation (Fig. 4, inset). In the plots of F_0/F *versus* $[Q]$, K_q is given by the ratio of the slope to the intercept. The K_q values of the two complexes are $1.2\times10^4\,\mathrm{M}^{-1}$ and $2.3\times10^4\,\mathrm{M}^{-1}$ for complex **1** and complex **2**, respectively. These results suggest that complex **2** is more capable than complex **1** at replacing the strong DNA intercalator EB, which are in accordance with the above absorption titration results.

CD Spectroscopy Circular dichroic spectral techniques may provide useful information on how the conformation of the CT-DNA chain is influenced by the bound complex. The CD spectrum of CT-DNA consists of a positive band at 274 nm that can be due to base stacking and a negative band at 243 nm that can be due to helicity and is also characteristic of DNA in a right-handed B form.[30] The changes in CD signals of CT-DNA observed on interaction with drugs may often be assigned to the corresponding changes in CT-DNA structure.[31] Thus simple groove binding and electrostatic interaction of small molecules show less or no perturbation on the base-stacking and helicity bands, whereas intercalation enhances the intensities of both the bands stabilizing the right-handed B conformation of CT-DNA as observed for the classical intercalator methylene blue.[32]

The CD spectra of DNA taken after incubation of the complexes with CT DNA are shown in Fig. 5. In all cases, the intensities of both the negative and positive bands decrease significantly. This suggests that the DNA binding of the complexes induces certain conformational changes, such as the conversion from a more B-like to a more C-like structure within the DNA molecule.[33—35] These changes are indicative of a non-intercalative mode of binding of these complexes and offer support to their groove binding nature.[36] The changing intensity follows the order of **2**>**1**.

Viscosity Studies Hydrodynamic measurements that are sensitive to the length change (*i.e.*, viscosity and sedimentation) are regarded as the least ambiguous and the most critical tests of a binding model in solution in the absence of crystallographic structural data. Viscosity studies were carried out as a means for further clarifying the binding of complex **1** with DNA, viscosity studies are carried out. Data are presented as $(\eta/\eta_0)^{1/3}$ *versus* $1/R$, where R=[DNA]/[compound]; and η and η_0 are the relative viscosities of DNA in the presence and absence of compound, respectively. The relative viscosity values are calculated from the flow time of DNA-containing solution (t) and the flow time of buffer alone (t_0), using the expression (5),[37]

$$\eta=(t-t_0)/t_0 \quad (5)$$

Intercalating agents are expected to elongate the double helix to accommodate the compounds in between the base leading to an increase in the viscosity of DNA. In contrast, complexes that bind exclusively in the DNA grooves by partial and/or non-classical intercalation, under the same conditions, typically cause less pronounced (positive or negative) or no change in DNA solution viscosity.[38] As a validation of the above verdict, viscosity measurements were carried out. The effects of the compounds together with EB on the viscosity of DNA at 25.0±0.1 °C are shown in Fig. 6. The results reveal that complexes **1** and **2** effect relatively inapparent increase in DNA viscosity, consistent with the DNA groove binding suggested above, which is also known to enhance DNA viscosity.[39] The increased degree of viscosity, which may depend on its affinity to DNA follows the order of **2**>**1**, which is consistent with our foregoing hypothesis.

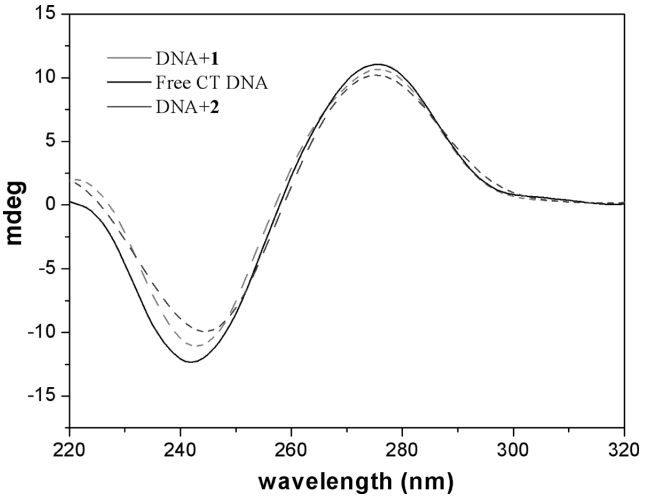

Fig. 5. CD Spectra of CT-DNA (120 μM) in the Absence or Presence of Complexes **1** and **2** (60 μM)

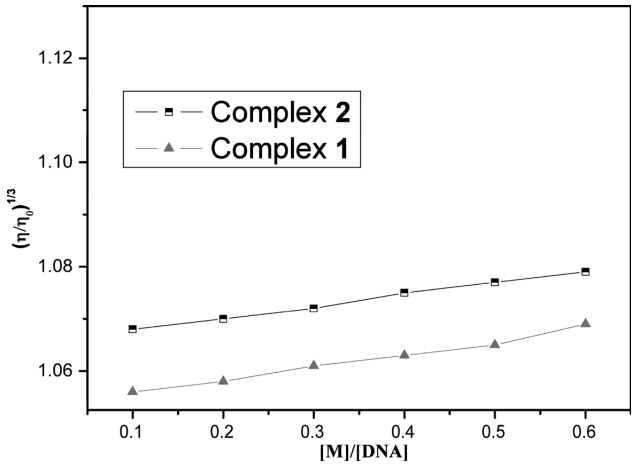

Fig. 6. Effect of Increasing Amounts of Complexes **1** and **2** on the Relative Viscosity of CT-DNA at 25 °C

[DNA]=50 μM, [complex]=1, 2, 3, 4, 5, 6 μM.

Scavenger Measurements of $O_2^{-\cdot}$ Figure 7a depicts the inhibitory effect of the compounds on $O_2^{-\cdot}$. The average suppression ratio for $O_2^{-\cdot}$ increases with the increase of the complex concentration in the range of tested concentrations. The average suppression ratio of the ligand metal salts can not be read. The Pr(III) complex **2** (IC_{50}=4.71±0.22 μM) is the most effective inhibitor in these complexes, whereas the Nd(III) complex **1** is the poorest one. The improvement of the complexes of the antioxidative properties of the Schiff base ligand may be explained by the redox behavior of the

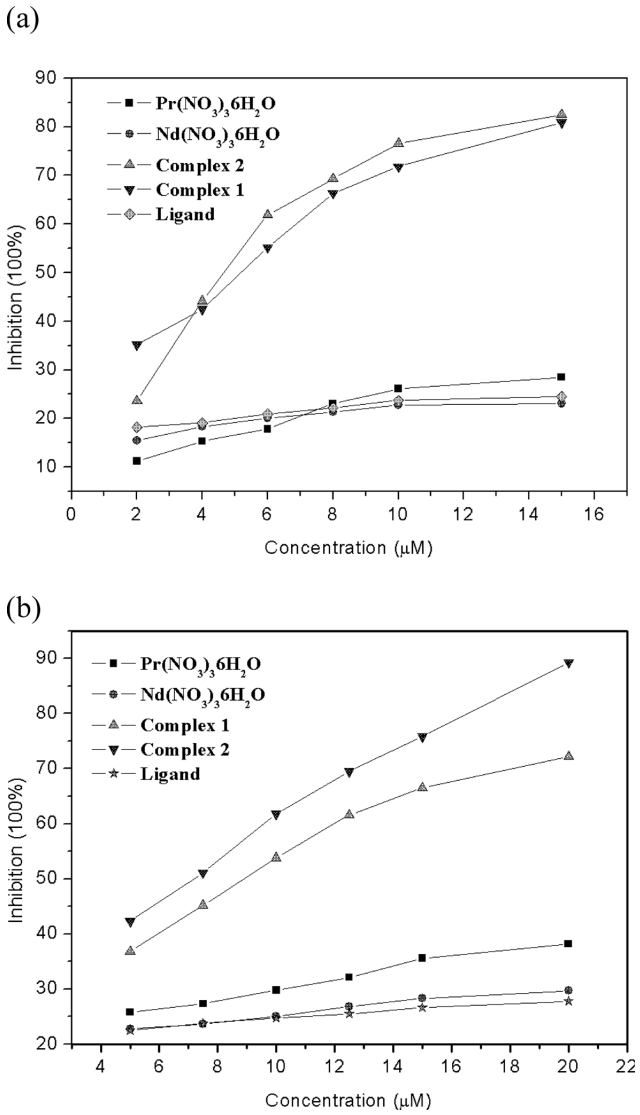

Fig. 7. (a) Effect of Tested Complexes **1** and **2** and Ligand on $O_2^{-\cdot}$ (b) Effect of Tested Complex **1** and Ligand on $OH^{\cdot}$

Experiments were performed in triplicate. Values are expressed as mean±standard deviation (n=3).

metal. The average suppression ratio of the metal salts is weaker than that of the corresponding complexes. It is clear that the scavenger effect on $O_2^{-\cdot}$ can be enhanced by the formation of metal–ligand complexes and the metal ions also affect the ability. Due to their lower values of IC_{50}, they are potential drugs to eliminate the radicals.

Hydroxy Radical Scavenging Activity The suppression ratio data for $OH^{\cdot}$ are shown in Fig. 7b. The inhibitory effect of the compounds is marked and the average suppression ratio for $OH^{\cdot}$ increases with an increase in compound concentration. The average suppression ratio of the Pr(III) complex (**2**) (IC_{50}=7.12±0.18 μM) is the most effective one. In addition, the average suppression ratio of the metal salts and ligand is weaker than that of the corresponding complexes, indicating that because of the formation of coordination compounds, the scavenger effect can be enhanced. Moreover, we found that complexes **1** and **2** are more effective inhibitors of $OH^{\cdot}$ than that of mannitol which is usually used as a special scavenger for $OH^{\cdot}$. Therefore, the metal complexes we studied in this paper are potential drugs for some diseases and therefore should be further researched.

Conclusion

In this paper, we have synthesized and characterized HL and its Pr(III) and Nd(III) complexes. In addition, the DNA-binding properties were investigated by electronic absorption, fluorescence, CD spectroscopy, and viscosity measurement. The results support the fact that complexes **1** and **2** can bind to CT-DNA by the mode of groove binding and the binding affinity of complex **2** is higher than that of complex **1**. Furthermore, the two complexes have active scavenging effects on $O_2^{-\cdot}$ and $OH^{\cdot}$. According to the IC_{50} values obtained, they are found to exert superior activity in comparison to the ligand HL. These findings clearly indicate that lanthanide-based complexes have many potential practical applications, such as the development of nucleic acid molecular probes and new therapeutic reagents for diseases.

Acknowledgements This work was supported by the State Key Laboratory of Applied Organic Chemistry, Lanzhou University.

References

1) Samanta B., Chakraborty J., Shit S., Batten S. R., Jensen P., Masuda J. D., Mitra S., *Inorganica Chimica Acta*, **360**, 2471—2484 (2007).
2) Rao S., Mishra D. D., Mourya R. V., Nageswara N., *Polyhedron*, **16**, 1825 (1999).
3) West D. X., Liberta A. E., Padhye S. B., Chikate R. C., Sonawane P. B., Umbhar A. S., Yerande R. G., *Coord. Chem. Rev.*, **123**, 49 (1993).
4) Martin R. B., Richardson F. S., *Q. Rev. Biophys.*, **12**, 181—209 (1979).
5) Laufer R. B., *Chem. Rev.*, **87**, 901—927 (1987).
6) Shibasaki M., Sasai H., Arai T., *Angew. Chem. Int. Ed. Engl.*, **36**, 1236—1256 (1997).
7) Xu H., Liang Y., Zhang P., Pu F., Zhou B. R., Wu J., Liu J. H., Liu Z. G., Ji L. N., *J. Biol. Inorg. Chem.*, **10**, 529—538 (2005).
8) Song Y. M., Wu Q., *J. Inorg. Biochem.*, **100**, 1685—1691 (2006).
9) Dilworth J. R., *Coord. Chem. Rev.*, **21**, 29—62 (1976).
10) Merchant J. R., Clothia D. S., *J. Med. Chem.*, **13**, 335—336 (1970).
11) Huang C. Z., Li Y. F., Feng P., *Talanta*, **55**, 321—328 (2001).
12) SMART and SAINT Software Reference Manuals, Versions 5.6 and 6.4, Bruker AXS, Madison, 2003.
13) Sheldrick, GM SADABS Software for Empirical Absorption Correction, University of Göttingen, Germany, 2003.
14) Sheldrick, G. M. SHELXS-97, A Program for X-ray Crystal Structure Solution and SHELXL-97, A Program for X-ray Structure Refinement, University of Göttingen, Germany, 1997.
15) Maurya M. R., Khurana S., Zhang W. J., Rehder D., *J. Chem. Soc., Dalton Trans.*, **15**, 3015—3023 (2002).
16) Marta G. A., Gloria A., Joaquín B., Lucas D. C. A., Santiago G. G., José M. M. B., *Inorg. Chem.*, **44**, 9424—9433 (2005).
17) Winterbourn C. C., *Biochem. J.*, **182**, 625—628 (1979).
18) Sharma S. D., Rajor H. K., Chopra S., Sharma R. K., *BioMetals*, **18**, 143—154 (2005).
19) Li T. R., Yang Z. Y, Wang B. D., *Chem. Pharm. Bull.*, **55**, 26—28 (2007).
20) Winterbourn C. C., *Biochem. J.*, **198**, 125—131 (1981).
21) Lewis F. D., Barancyk S. V., *J. Am. Chem. Soc.*, **111**, 8653—8661 (1989).
22) Raman N., Kulandaisamy A., Jeyasubramanian K., *J. Ind. Chem.*, **41A**, 942—949 (2002).
23) Mudasir, Yoshioka N., Inoue H., *J. Inorg. Biochem.*, **77**, 239—247 (1999).
24) Cory M., McKee D. D., Kagan J., Henry D. W., Miller J. A., *J. Am. Chem. Soc.*, **107**, 2528—2536 (1985).
25) Waring M. J., *J. Mol. Biol.*, **13**, 269—282 (1965).
26) Vaidyanathan V. G., Nair B. U., *J. Inorg. Biochem.*, **94**, 121—126 (2003).
27) Xi P. X., Xu Z. H., Liu X. H., Chen F. J., Liang Huang L., Zeng Z. Z. *Chem. Pharm. Bull.*, **56**, 541—546 (2008).
28) Indumathy R., Radhika S., Kanthimathi M., Weyhermuller T., Nair B.

U., *J. Inorg. Biochem.*, **101**, 434—443 (2007).
29) Efink M. R., Ghiron C. A., *Anal. Biochem.*, **114**, 199—227 (1981).
30) Ivanov V. I., Minchenkova L. E., Schyolkina A. K., Poletayer A. I., *Biopolymers*, **12**, 89—110 (1973).
31) Lincoln P., Tuite E., Norden B., *J. Am. Chem. Soc.*, **119**, 1454—1455 (1997).
32) Norden B., Tjerneld F., *Biopolymers*, **21**, 1713—1734 (1982).
33) Vaidyanathan V. G, Nair B. U., *Biochim. Biophys. Acta*, **1475**, 157—162 (2000).
34) Wang B. D., Yang Z. Y., Qin D. D., Chen Z. N., *J. Photochem. Photobiol. A Chem.*, **194,** 49—58 (2008).
35) Song Y. M., Wu Q., Yang P. J., Luan N. N., Wang L. F., Liu Y. M., *J. Inorg. Biochem.*, **100**, 1685—1691 (2006).
36) Vaidyanathan V. G., Vijayalakshmi R., Subramanain V., Nair B. U., *Bull. Chem. Soc. Jpn.*, **75**, 1143—1149 (2002).
37) Cohen G., Eisenberg H., *Biopolymers*, **8**, 45—55 (1969).
38) Liu C. S., Zhang H., Chen R., Shi X. S., Bu X. H., Yang M., *Chem. Pharm. Bull.*, **55**, 996—1001 (2007).
39) Selvi P. T., Palaniandavar M., *Inorg. Chim. Acta*, **337,** 420—428 (2002).